MITSUBISHI ELECTRIC RESEARCH LABORATORIES
http://www.merl.com

TOA Estimation with Different IR-UWB Transceiver Types

Ismail Guvenc, Zafer Sahinoglu

TR2005-131 December 2005

Abstract

In this paper, performances of stored-reference (SR), transmitted-reference (TR), and energy detection (ED) based time of arrival (TOA) estimation techniques are analyzed for impulse-radio ultra-wideband (IR-UWB) systems. Various maximum likelihood estimation approaches are investigated under different observation models, and a new estimator that exploits the noise statistics and power delay profile of the channel is proposed. Simulation results show that ED and TR perform well if the sampling rate is much smaller than the Nyquist rate. Also, exploiting the channel and noise statistics considerably improves the accuracy of peak selection.

IEEE International Conference on Ultrawideband, Sept. 2005

TOA Estimation with Different IR-UWB Transceiver Types

Ismail Guvenc[1,2] and Zafer Sahinoglu[1]
[1]Mitsubishi Electric Research Labs, 201 Broadway Ave., Cambridge, MA, 02139
[2]Department of Electrical Engineering, University of South Florida, Tampa, FL, 33620
E-mail:{guvenc, zafer}@merl.com

***Abstract*— In this paper, performances of stored-reference (SR), transmitted-reference (TR), and energy detection (ED) based time of arrival (TOA) estimation techniques are analyzed for impulse-radio ultra-wideband (IR-UWB) systems. Various maximum likelihood estimation approaches are investigated under different observation models, and a new estimator that exploits the noise statistics and power delay profile of the channel is proposed. Simulation results show that ED and TR perform well if the sampling rate is much smaller than the Nyquist rate. Also, exploiting the channel and noise statistics considerably improves the accuracy of peak selection.**

I. Introduction

Ultra-wideband (UWB) is a technology that has distinct features characterized by its extremely wide bandwidth. Due to the high time resolution of the received signal, it is possible to accurately identify the first arriving impulse radio (IR)-UWB signal path, which may not be the strongest. Precision ranging is achieved by leading edge detection of the received samples using appropriate algorithms. However, due to the large bandwidths employed on the order of gigahertz, typical UWB receivers can not operate at Nyquist rate. Instead, energy can be captured at lower sampling rates after certain analog front-end processing and using different transceiver architectures.

The energy detection (ED) of the signal is achieved by passing the signal through a square-law device, followed by an integrator and sampler. On the other hand, the signal can be correlated via a stored-reference (SR) before integrate and dump circuitry, which is more robust to noise effects due to noise-free template employed. In order to avoid timing and pulse-shape mismatch between the reference template and received signal, a transmitted-reference (TR) can also be considered, where a reference template accompanies and matches to the transmitted data signal with a known delay in between. The low-rate digital samples obtained with either of ED, SR or TR are then processed for leading edge detection of the IR-UWB signal.

Typical approaches for UWB time of arrival (TOA) estimation in the literature are based on Nyquist rate (or close to Nyquist rate) sampling of the signal [1], [2], using an SR [3], [4], and using an ED [4], [5]. Once the samples are collected using these schemes, algorithms such as threshold comparison (TC) [6], [7], maximum energy selection (MES) [3], [5], [8]-[10], or their combination [1], [11] are applied to the samples for leading edge detection. Techniques for improving the accuracy of MES are introduced in [11], while optimal threshold estimation techniques are discussed in [6]. Tian *et. al.* successfully applies *data-aided* Generalized likelihood ratio testing for acquisition of UWB signals in [12], where noisy templates deduced from consecutive symbols are used that asymptotically approaches ideal templates for very large number of training symbols. Method of moments estimator was used in [4] for evaluating the parameters of the likelihood function in a multiple hypothesis testing formulation, which may be computationally costly. Trade-off's between stored-reference and transmitted-reference transceiver types for symbol detection was addressed in [13].

The performance trade-off's between different transceiver architectures for UWB ranging are not addressed in the literature to the best knowledge of the authors. In this paper, SR, TR, and ED based TOA estimation schemes are analyzed, their statistics are discussed, and performances are compared via simulations. Multiple hypothesis testing techniques are investigated. A Bayesian algorithm that gives a lower bound is presented, and maximum likelihood techniques based on different observation models and with various complexity levels are introduced. The analysis shows that when under-sampled signal is considered, SR is more susceptible to timing mismatches compared to TR and ED.

II. System Model

While the transmitted signals are the same for SR and ED receivers, TR includes delayed version of the same signal, and therefore yielding a slightly different transmitted signal model. Let the received UWB multipath signal for the former schemes be represented as

$$r(t) = \underbrace{\sum_{j=-\infty}^{\infty} d_j \omega_{mp}\big(t - jT_f - c_j T_c - \tau_{toa}\big)}_{r_s(t)} + n(t) \ , \quad (1)$$

while for the TR case the received signal is modeled by[1]

$$\tilde{r}(t) = \frac{1}{\sqrt{2}}\big(r_s(t) + r_s(t-D)\big) + n(t) \ , \quad (2)$$

where frame index and frame duration are denoted by j and T_f, N_s represents the number of pulses per symbol, T_c is the chip duration, T_s is the symbol duration, τ_{toa} is the TOA of the received signal, and N_h is the possible number of chip positions per frame, given by $N_h = T_f/T_c$. Effective pulse after the channel impulse response is given by $\omega_{mp}(t) = \sqrt{E}\sum_{l=1}^{L} \alpha_l \omega_l(t-\tau_l)$, where $\omega_l(t)$ is the received UWB pulse at lth tap with unit energy, E is the pulse energy, α_l and τ_l are the fading coefficients and delays of the multipath components, respectively. Additive white Gaussian noise (AWGN) with zero-mean and double-sided power spectral density $\mathcal{N}_0/2$ and variance σ^2 is denoted by $n(t)$. The delay between the data and

[1]Even though we refer the pair of signals in TR as reference and data signals, this is just for the sake of distinction, and we consider no data modulation for ranging purposes.

0-7803-9398-8/05/$20.00 ©2005 IEEE

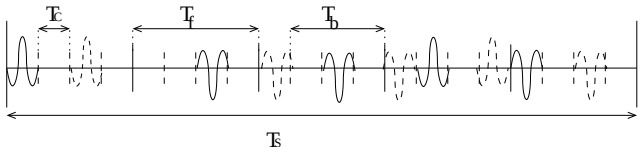

Fig. 1. Illustration of transmitted IR-UWB pulses in a symbol, where $(N_s, N_h) = (5, 4)$, $T_b = 3T_c$, and $(\{c_j\}, \{d_j\}) = (\{0, 2, 1, 1, 0\}, \{+1, -1, -1, +1, -1\})$. The pulses with solid lines correspond to ED and SR. Dashed pulses can be included for TR (after appropriate energy scaling) with $D = 2T_c$.

reference signals is denoted by D, and energy is appropriately scaled so that energy per symbol is identical for all cases. No modulation is considered for the ranging process. In order to avoid catastrophic collisions, and smooth the power spectral density of the transmitted signal, time-hopping codes $c_j^{(k)} \in \{0,\ 1, ..., N_h - 1\}$ are assigned to different users. Moreover, random-polarity codes $d_j \in \{\pm 1\}$ are used to introduce additional processing gain for the detection of desired signal, and smooth the signal spectrum (see Fig. 1).

A. Sampling the Received Signal After Different Energy Collection Techniques

The signal arriving at the receiver's antenna is passed through a low noise amplifier (LNA) and a band pass filter (BPF) of bandwidth B. Different approaches for collecting the energy are possible before sampling the signal in (1) or (2). The received signal can be sampled after a square-law device (Fig. 2a), after correlation with a stored-reference signal (Fig. 2b), or after correlation with a transmitted-reference signal (Fig. 2c). Block duration (which depends on the sampling interval) is denoted by T_b, and can be the taken as T_c for chip-spaced sampling. In the sequel, we assume that a coarse acquisition on the order of frame-length is acquired in (1), such $\tau_{toa} \sim \mathcal{U}(0, T_f)$, where $\mathcal{U}(.)$ denotes the (continuous) uniform distribution. The signal within time frame T_f plus half of the next frame is sampled and searched to factor-in inter-frame leakage due to multipath. The number of samples (or blocks/chips) is denoted by $N_b = \frac{3}{2}\frac{T_f}{T_b}$, and $n \in \{1, 2, ..., n_{toa}, ..., N_b\}$ denotes the sample index with respect to the starting point of the uncertainty region.

With a sampling interval of t_s, the sample values at the output of the square-law device are given by

$$z_n^{(ed)} = \sum_{j=1}^{N_s} \int_{(j-1)T_f+(c_j+n-1)t_s}^{(j-1)T_f+(c_j+n)t_s} |r(t)|^2 dt \ , \qquad (3)$$

while the stored-reference template signal and the samples after correlating the received signal with this template are given by,

$$s_{tmp}(t) = \sum_{j=0}^{N_s-1} d_j \omega\big(t - jT_f - c_j T_c\big) \ , \qquad (4)$$

$$z_n^{(sr)} = \int_{(n-1)t_s}^{(n-1)t_s+N_s T_f} r(t) s_{tmp}\big(t - (n-1)t_s\big) dt \ , \qquad (5)$$

respectively, where ω denotes the correlator pulse shape[2]. The samples after correlating with the delayed version of the signal

[2]Note that since received pulse shape ω_l can change at different multipath components, ω will not typically match with the received pulse shapes. However, we have used $\omega = \omega_l$ for all l in the simulations for simplicity.

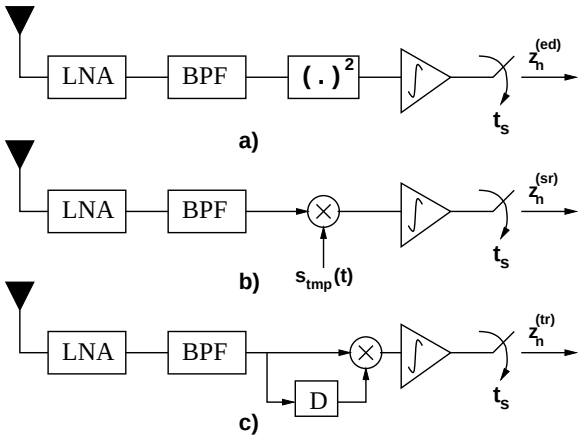

Fig. 2. Sampling of the received signal after a) Energy detection, b) Correlation with a local reference, and c) Correlation with a transmitted reference.

itself is formulated as

$$z_n^{(tr)} = \sum_{j=1}^{N_s} \int_{(j-1)T_f+(c_j+n-1)t_s}^{(j-1)T_f+(c_j+n)t_s} \tilde{r}(t)\tilde{r}(t - D) dt \ , \qquad (6)$$

and the performance can be further improved in all cases by transmitting multiple symbols.

B. Trade-off's Between Different Transceiver Architectures

It is very well known that matched filtering, where a stored reference signal is correlated with the received signal, is optimal detection technique when the knowledge of the received waveform shape is available. However, Nyquist-rate sampling is essential to match with the received signal, so that perfect alignment with the template and received waveform can be obtained. If only lower sampling rates are possible, it is apparent from (5) that SR will not be able to collect sufficient energy from the received multipath arrivals due to the timing (as well as pulse-shape) mismatches between the stored template signal and the received waveform.

On the other hand, ED and TR signaling can both effectively capture the received energy. Even with low sampling rates, neither non-coherent schemes require the knowledge of the timings or pulse shapes, which are perfectly available (assuming accurate delay lines for the TR case). The existence of the transmitted-reference pulse yields a 3dB transmitted energy loss compared with the other two schemes. Illustration of the timing susceptibility for SR, TR, and ED are presented in Fig. 3. If sufficient sampling rate is available, SR will better characterize the peak; however, with low sampling rates (e.g. $<$ 1ns), it is more likely that SR will loose the peak completely.

The serious problem with both the non-coherent approaches is the enhanced noise terms in the low SNR region. In particular, noise-square terms for the ED, and noise-cross-noise terms for TR seriously dominate and degrade the detection performance. Therefore, even though non-coherent approaches outperform SR at high SNR due to better energy capture (with moderate sampling rates), they have poor performance when the noise variance is large. Due to similar reasons, TR and ED are much more susceptible to interference compared to SR. In Fig. 4, the energy statistics are depicted and summarized for

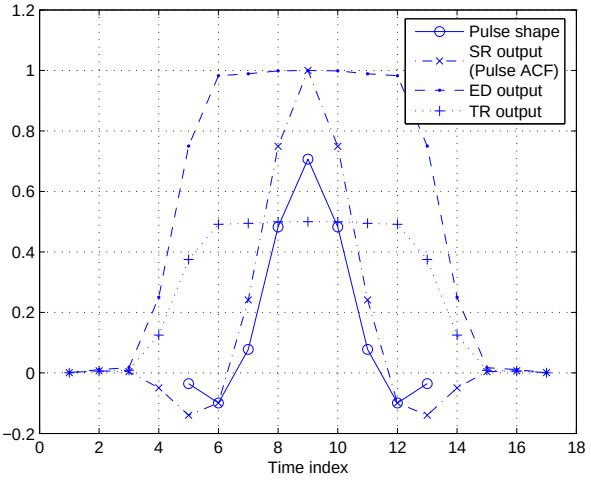

Fig. 3. Received *normalized* pulse shape, and the sampled outputs corresponding to SR, ED, and TR for different timing offsets (1ns pulse is sampled at 8GHz, and energy is collected within 1ns windows and different offsets). The ED and TR outputs will scale with E, while SR output will scale with $\sqrt{E}$ for different E_b/N_0.

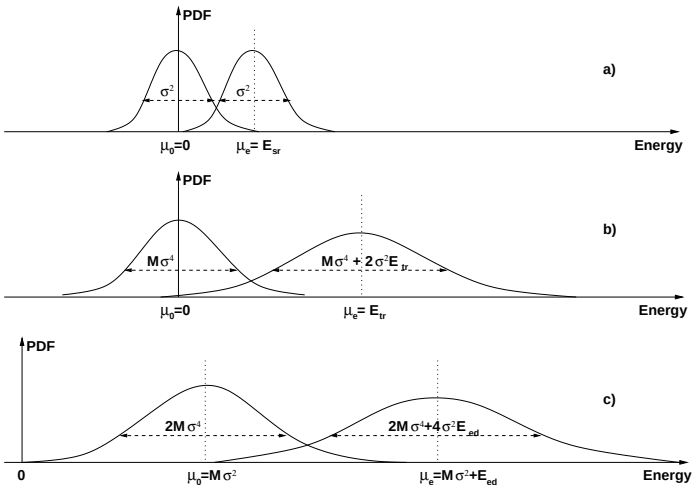

Fig. 4. Comparison of mean and variance statistics of the sampled received signal in the presence and absence of signal energy within a certain sampling interval: a) Stored-reference, b) Transmitted-reference, c) Energy detection. Note that for accurate timing, $E_{ed} = 2E_{tr} = E_{sr}^2 = E$, while while for timing mismatches, $E_{ed} = 2E_{tr} > E_{sr}$ (assuming accurate delay lines for TR).

the three approaches for a given time interval[3]. It is observed that noise variance seriously increases for the non-coherent approaches, while the ED achieves the best energy collection.

Comparing the transmitted waveforms, TR has a longer time span compared to ED and SR, and D has to be large enough so that multipath interference between reference and data pulses is not a serious problem. Also, TR observes enhanced early/late (E/L) noise terms that arise when either the reference or data signal samples are correlated with the noise-only samples. This scales the noise variance at $\pm D$ of the actual TOA by the signal energy.

III. Multiple Hypothesis Testing for TOA Estimation

Once the received signal is sampled, and leading edge of the signal lies within an interval of samples, TOA estimation can be achieved by a *multiple hypothesis testing* (MHT), and by choosing the hypothesis that maximizes the likelihood function [14]. Based on the observation model, and amount of *a priori* information available about the received signal (channel statistics, noise variance etc.), different TOA estimators can be defined. In this section, maximum likelihood estimators with different complexity levels will be presented. Also, Bayesian detection that gives a theoretical lower bound on the TOA estimate will be introduced. In order to have a unified analysis, the absolute values of the samples in (5) and (6) are used[4], denoted by a common notation z_n for any of the three schemes. Also, ED will be taken as a case study to define the signal statistics; however, similar analysis can be carried out for the other two schemes.

[3]The scales are adjusted for the sake of illustration and comparison between different schemes, and only comparatively represents actual scaling.

[4]Which actually changes statistics after the sampler of SR and TR in Fig. 4. Since no channel estimate is available at ranging step, it is not possible to coherently process SR samples.

A. Problem Formulation

Let $\underline{z}$ denote the $1 \times N_b$ vector of samples z_n, N_e denote the number of signal plus noise energy samples, $\underline{z}_k^{(no)}$ and $\underline{z}_k^{(sn)}$ denote (for the kth hypothesis) the noise-only energy vector and signal plus noise energy vector of sizes $1 \times (N_b - N_e)$ and $1 \times N_e$, respectively, where vectors on the two sides of signal plus noise vector $\underline{z}_k^{(sn)}$ are concatenated to yield $\underline{z}_k^{(no)}$. Consider an ED with $N_s = 1$ and no time hopping, and let $T_b = t_s$. Then, following multiple hypothesis testing can be considered for $k = 1, 2, ..., N_b$

$$\begin{aligned} \mathcal{H}_k: \quad & z_n = \textstyle\int_{(n-1)T_b}^{nT_b} \eta^2(t)dt, && n = 1, ..., k-1 \\ & z_n = \textstyle\int_{(n-1)T_b}^{nT_b} \left[r_s(t) + \eta(t)\right]^2 dt, && n = k, ..., k+N_e-1 \\ & z_n = \textstyle\int_{(n-1)T_b}^{nT_b} \eta^2(t)dt, && n = k+N_e, ..., N_b \end{aligned} \tag{7}$$

where $\eta(t)$ is the noise after the BPF (signal part is assumed to be undistorted due to BPF). Using the Chi-square statistics that arise due to square-law device, (7) becomes

$$\begin{aligned} \mathcal{H}_k: \quad & z_n = \chi(M), && n = 1, ..., k-1 \\ & z_n = \chi(E_n, M), && n = k, ..., k+N_e-1 \\ & z_n = \chi(M), && n = k+N_e, ..., N_b \end{aligned} \tag{8}$$

where Chi-square random variable is denoted with χ, with parameter M for the centralized, and parameters (E_n, M) for non-centralized cases, respectively. The degree of freedom of the noise terms is denoted by $M = 2Bt_s + 1$. The signal energy in the nth block is denoted by E_n, which has a different distribution in different blocks. For notational convenience, define index $m \in \{1, 2, ..., N_e\}$ for the signal plus noise energy vector for the range of $k \le n \le k + N_e - 1$, where $m = n - k + 1$, and $\mathcal{E}_m = E_n$. Gaussian approximation can be used to model z_n for large enough M, where the means and variances become $\mu_n = M\sigma^2$, $\sigma_n^2 = 2M\sigma^4$ for the centralized, and $\mu_n = M\sigma^2 + E_n$, $\sigma_n^2 = 2M\sigma^4 + 4\sigma^2 E_n$ for the non-centralized Chi-square distributions.

B. Maximum Likelihood Estimation

Probably the simplest way of achieving the leading energy block estimate is maximum energy selection (MES) from the individual energy samples, which yields $\hat{n}_{toa} = \underset{k\in\{1,\ldots,N_b\}}{\text{argmax}} \left\{z_k\right\}$. However, MES is susceptible to noise since the energy in only a single sample is used, and it does not provide high timing resolution as there may be a large delay between the leading edge and the maximum energy block (as much as 60ns for CM1). In order to exploit the energy in the neighboring multipath components, energy samples can be summed within a window, and the leading block estimate using maximum energy sum selection (MESS) is given by $\hat{n}_{toa} = \underset{k\in\{1,\ldots,N_b\}}{\text{argmax}} \left\{\underline{z}_k^{(sn)} \times \underline{1}_{N_e}\right\}$, which is similar conceptually to the synchronization algorithm in [5] except the window definitions and signaling schemes.

If some *a-priori* knowledge about the channel power delay profile is available, it can be used to weight the hypothesized energy vector, which yields $\hat{n}_{toa} = \underset{k\in\{1,\ldots,N_b\}}{\text{argmax}} \left\{\underline{z}_k^{(sn)} \times \underline{\rho}_{N_e}\right\}$, where $\underline{\rho}_{N_e}$ is the exponentially decaying column vector of $1 \times N_e$ mean energies for a particular channel model and block duration (see Fig. 5, where even though the normalized channel impulse responses of both channel models have unit energy, the signal energy after convolved with a pulse considerably decreases for CM2 due to its dispersive nature and inter-pulse interference). This weighted-MESS (W-MESS) is actually identical to correlating the received energy vector with the mean energy values before peak selection.

In addition that the captured energy is maximized, for the case of accurate hypothesis selection, the noise parameters $\hat{\mu}_k^{(no)}$ and $\hat{\sigma}_k^{(no)}$ will also be minimized. Therefore, weighting the energy sum in W-MESS with the inverse of these parameters will increase the accuracy, where the TOA estimate for W_2-MESS becomes

$$\hat{n}_{toa} = \underset{k\in\{1,\ldots,N_b\}}{\text{argmax}} \left\{ \frac{\underline{z}_k^{(sn)} \times \underline{\rho}_{N_e}}{\hat{\mu}_k^{(no)} \times \hat{\sigma}_k^{(no)}} \right\} . \tag{9}$$

Note that for both W-MESS and W_2-MESS, even if the power delay profile is not exactly available, an appropriate exponential can be used to weight the energy vector to enhance the performance of the MES.

C. Generalized Maximum Likelihood Estimation

The generalized maximum likelihood (GML) estimate of the leading energy block requires estimation of the statistical parameters at each sample. Using the Gaussian approximation of the Chi-square statistics, GML estimate is given by

$$\hat{n}_{toa} = \underset{k\in\{1,\ldots,N_b\}}{\text{argmax}} \left\{ p(\underline{z}\,|k, \underline{\hat{\mu}}_k, \underline{\hat{\sigma}}_k) \right\} , \tag{10}$$

where $\underline{\hat{\mu}}_k = [\hat{\mu}_k^{(no)}, \hat{\mu}_{k,1}^{(sn)}, ..., \hat{\mu}_{k,N_e}^{(sn)}]$, $\underline{\hat{\sigma}}_k = [\hat{\sigma}_k^{(no)}, \hat{\sigma}_{k,1}^{(sn)}, ..., \hat{\sigma}_{k,N_e}^{(sn)}]$ are the maximum likelihood estimates (MLE) of mean and standard deviation vectors of size $1 \times (N_e + 1)$ each, which maximize the likelihood function for the kth hypothesis. Therefore, GML estimation requires $2(N_e + 1)$ parameters to be estimated for *each hypothesis*[5].

[5]In fact, using the dependencies between the mean and variance parameters, estimation of $\underline{\mathcal{E}}$ and σ^2 is sufficient, yielding $N_e + 1$ parameters to be estimated.

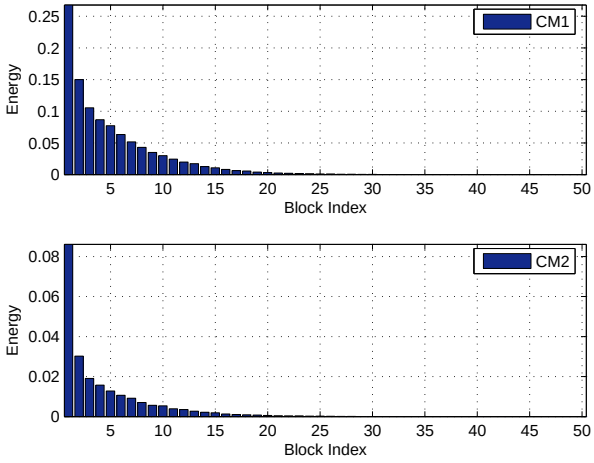

Fig. 5. Mean block energy with respect to block index (averaged over 1000 CM1 and CM2 channel realizations, $T_b = 4$ns, with random path offset).

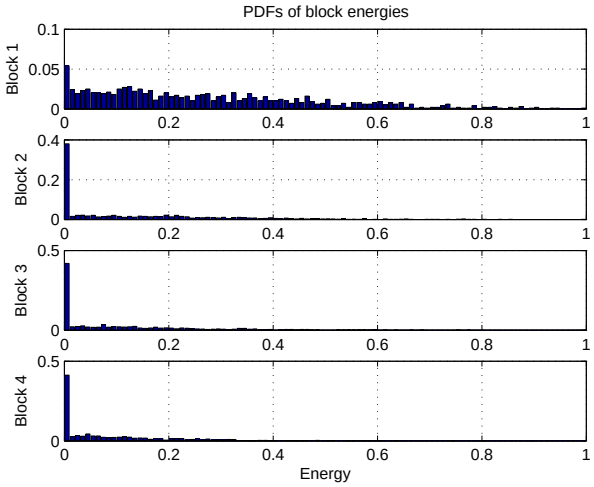

Fig. 6. PDFs of energies in blocks 1 through 4 (averaged over 1000 realizations of CM1, $T_b = 4$ns, $T_c = 1$ns, with random path offset).

The MLEs for the noise-only vector parameters are evaluated as $\hat{\mu}_k^{(no)} = \frac{1}{N_b - N_e} \underline{z}_k^{(no)} \times \underline{1}_{N_b - N_e}$, and $\hat{\sigma}_k^{(no)} = \frac{1}{N_b - N_e} \left[(\underline{z}_k^{(no)} - \hat{\mu}_k^{(no)})(\underline{z}_k^{(no)} - \hat{\mu}_k^{(no)})^T \right]^{1/2}$, respectively, where $\underline{1}_\nu$ is a column vector of size ν. The MLE of the parameters for the signal plus noise energy blocks can be obtained by assuming that $\underline{z}_k^{(sn)}$ decays exponentially on the average (see Fig. 5). However, for individual channel realizations, there will be multiple clusters, and forcing a single-exponential fit to the received samples yields a modeling error (as will be observed in simulation results). Nevertheless, the mean corresponding to each hypothesis of signal plus noise vector can be modeled by an exponential of the form $\hat{\mu}_{k,m}^{(sn)} = A_{1,k} \exp(-A_{2,k} m) + A_{3,k}$, where $A_{3,k} = \hat{\mu}_k^{(no)}$ and is estimated from hypothesized noise-only blocks. Parameter A_2 may be assumed fixed (knowing the channel model), which yields a low-complexity exponential fit to the data (GML-v1). Alternatively, A_2 can be jointly estimated with A_1, which is computationally more complex (GML-v2). Once the mean

energies are estimated, in order to calculate the standard deviation for each block (which are required for calculating the likelihood function in (10) using the Gaussian approximation), the following simple relationships can be used: $\hat{\mu}_{k,m}^{(sn)} = M\sigma^2 + \hat{\mathcal{E}}_m = \hat{\mu}_k^{(no)} + \hat{\mathcal{E}}_m$, $\hat{\sigma}_{k,m}^{(sn)} = \left(2M\sigma^4 + 4\sigma^2\hat{\mathcal{E}}_m\right)^{\frac{1}{2}} = \left([\hat{\sigma}_k^{(no)}]^2 + 4\frac{\hat{\mu}_k^{(no)}}{M}\hat{\mathcal{E}}_m\right)^{\frac{1}{2}}$, where $\hat{\mathcal{E}}_m$ from the first equality can be plugged into the second equality, yielding

$$\hat{\sigma}_{k,m}^{(sn)} = \left([\hat{\sigma}_k^{(no)}]^2 + 4\frac{\hat{\mu}_k^{(no)}}{M}\left(\hat{\mu}_{k,m}^{(sn)} - \hat{\mu}_k^{(no)}\right)\right)^{\frac{1}{2}} . \qquad (11)$$

D. Bayesian Estimation

If the distribution of $\mathcal{E}_m$ are known *a-priori* for each energy block m, and noise variance σ^2 is known exactly (both of which are extremely difficult in most cases), an *optimal* solution can be developed using a Bayesian approach. The leading energy block estimate in this case is given by

$$\hat{n}_{toa} = \underset{k\in\{1,\ldots,N_b\}}{\operatorname{argmax}} \left\{ \int_{\mathcal{E}_1}\int_{\mathcal{E}_2}\ldots\int_{\mathcal{E}_{N_e}} p(\underline{z}\,|k,\sigma,\underline{\mathcal{E}}) \times p(\mathcal{E}_1)\ldots p(\mathcal{E}_{N_e}) d\mathcal{E}_{N_e}\ldots d\mathcal{E}_1 \right\} , \qquad (12)$$

where $\underline{\mathcal{E}} = [\mathcal{E}_1, \mathcal{E}_2, \ldots, \mathcal{E}_{N_e}]$ is the vector of signal energies in the signal plus noise blocks. Distributions of normalized energies within 100 discrete bins in $(0,1)$ are presented in Fig. 6 for CM1, and it is desirable to choose N_e on the order of maximum excess delay to have accurate estimates. Since it is usually very hard to know the prior PDFs of the parameters, and it requires multidimensional integration over the PDF of each parameter yielding a very complex implementation, Bayesian analysis is usually of theoretical interest rather than practical consideration.

IV. Simulation Results

Computer simulations are performed to evaluate the introduced TOA estimation techniques. The channel models CM1 (residential LOS) and CM2 (residential NLOS) of IEEE802.15.4a are employed. The channel realizations are sampled at 8GHz, 1000 different realizations are generated, and each realization has a TOA uniformly distributed within $(0, T_f)$. A raised cosine pulse of $T_c = 1$ns is considered for all scenarios. After introducing uniformly distributed delays, energies are collected within non-overlapping windows to obtain decision statistics. The other simulation parameters are (unless otherwise stated) $T_f = 200$ns, $B = 4$GHz, $N_s = 1$, and only a single ranging symbol is used. Both 1ns and 4ns are considered for T_b, with corresponding N_e of 100 and 24, respectively, so that significant multipath energy can be captured. For all the simulations the TOA estimate is taken to be the center of the block estimate, and timing errors are averaged over 1000 different channel realizations.

Two scenarios are considered for the leading edge path within the first energy block. The first scenario assumes that there is no offset within the first energy block, and stored reference has at least accurate timing with the first chip that includes the signal. On the other hand, in the second scenario, the first path may arrive anywhere within the first signal block. The cumulative distribution function (CDF) of the delays between the maximum energy sample and the leading edge sample are compared for different transceiver types in Fig. 7 for both scenarios. While choosing the peaks yields a closer timing to the leading edge for SR for the first scenario, ED and TR has better characteristics at low sampling rates when no first-path synchronization is assumed.

Performances of ED, SR, and TR are compared in Figs. 8-10, when MES and threshold comparison (TC) is employed for CM1 and CM2. Threshold comparison chooses the first threshold exceeding sample, where threshold is defined as $0.5\big(\min(z_n)+\max(z_n)\big)$. It is seen that when MES and TC are used, SR performs better only if synchronization to the first path is assumed. Performance difference between CM1 and CM2 decreases with E_b/N_0 in favor of CM2, and the error-floor performances are better for CM2, which can be explained with the fact that the distance between the maximum energy block and leading edge block is smaller for CM2 [6].

The mean absolute errors (MAE) of the TOA estimates for different algorithms in CM1 are presented in Fig. 11 for ED ($T_b = 4$ns). The Bayesian estimation, which is obtained using histograms of discrete bins, yields a lower bound at high E_b/N_0. The Bayesian estimate not being as good at low E_b/N_0 may be explained with small number of samples available (which may be insufficient to be modeled via the PDFs), and the inaccuracy of the Gaussian approximation of Chi-square statistics (where $M = 32$ from simulation parameters). Despite its computational complexity, even though it is better than MES at most of the E_b/N_0 region, and *it does not require* knowledge of channel statistics, GML suffers from a modeling error. At low E_b/N_0, multiple clusters of the arriving signal are buried in noise. However, when noise variance is smaller, GML forces an exponential fit to individual clusters, which even increases the timing error. On the other hand, W_2MESS significantly outperforms all the other practical algorithms, and has a reasonably low complexity, requiring power delay profile of the channel.

V. Conclusion

In this paper, TOA estimation techniques for impulse radio UWB systems based on multiple hypothesis testing are evaluated and compared for different transceiver architectures. Simulation results show that performance of peak selection can be enhanced by making use of channel information and noise statistics. Also, in order for stored-reference to have precise timing, high sampling rates are required so that the autocorrelation peak can be accurately captured.

Acknowledgement

The authors would like to thank Philip Orlik for useful discussions and for reviewing the paper.

References

[1] J.-Y. Lee and R. A. Scholtz, "Ranging in a dense multipath environment using an UWB radio link," *IEEE J. Select. Areas Commun.*, vol. 20, no. 9, pp. 1677–1683, Dec. 2002.

[2] C. Mazzucco, U. Spagnolini, and G. Mulas, "A ranging technique for UWB indoor channel based on power delay profile analysis," in *Proc. IEEE Vehic. Technol. Conf. (VTC)*, Los Angeles, CA, Sep. 2004, pp. 2595–2599.

[3] B. Denis, J. Keignart, and N. Daniele, "Impact of NLOS propagation upon ranging precision in UWB systems," in *Proc. IEEE Conf. Ultrawideband Syst. Technol. (UWBST)*, Reston, VA, Nov. 2003, pp. 379–383.

[4] S. Gezici, Z. Sahinoglu, H. Kobayashi, and H. V. Poor, *Ultra Wideband Geolocation*. John Wiley & Sons, Inc., 2005, in Ultrawideband Wireless Communications.

[5] A. Rabbachin and I. Oppermann, "Synchronization analysis for UWB systems with a low-complexity energy collection receiver," in *Proc. IEEE Conf. Ultrawideband Syst. Technol. (UWBST)*, Kyoto, Japan, May 2004, pp. 288–292.

[6] I. Guvenc and Z. Sahinoglu, "Threshold-based TOA estimation for impulse radio UWB systems," IEEE Int. Conf. UWB (ICU), Zurich, Switzerland, Sept. 2005, accepted for publication.

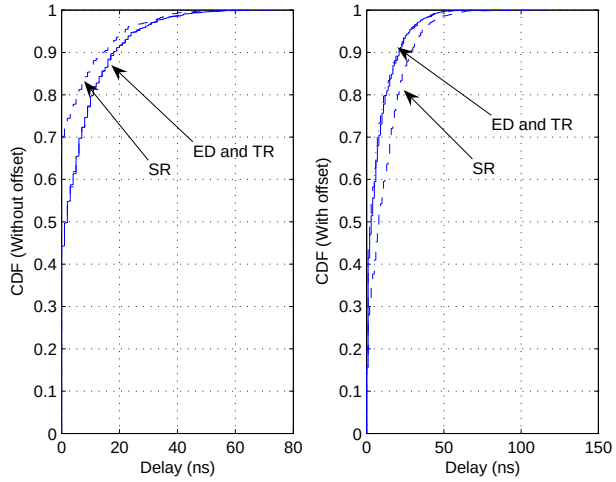

Fig. 7. CDFs of delays between peak and leading edge for SR, TR, ED ($t_s = T_b = 1$ns), and with and without path offsets within first energy block.

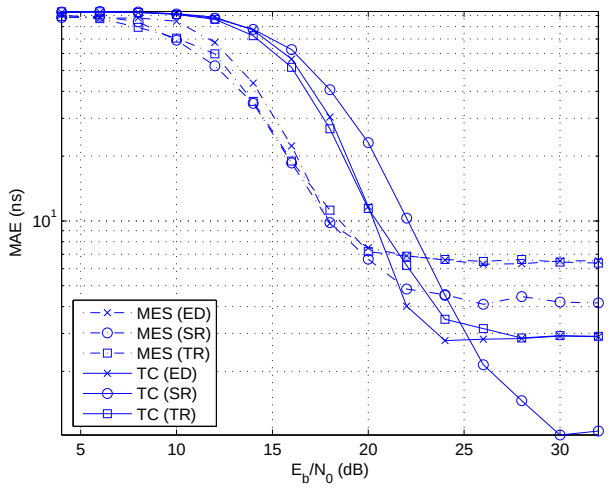

Fig. 8. TOA estimation performances of different transceiver types using MES and TC (CM1, $t_s = T_c = T_b = 1$ns), without timing offset within first energy block.

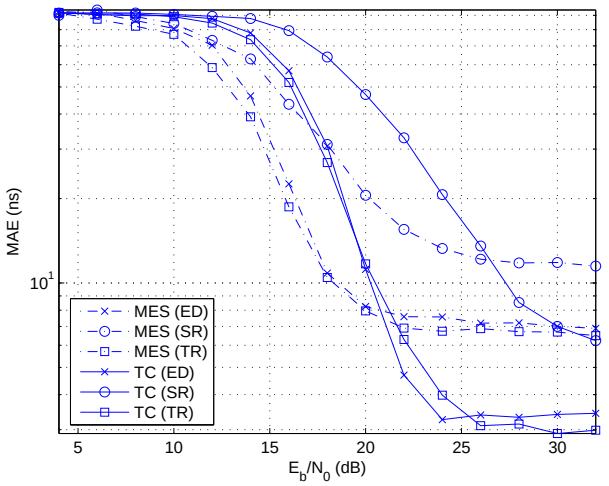

Fig. 9. TOA estimation performances of different transceiver types using MES and TC (CM1, $t_s = T_c = T_b = 1$ns), with timing offset within first energy block.

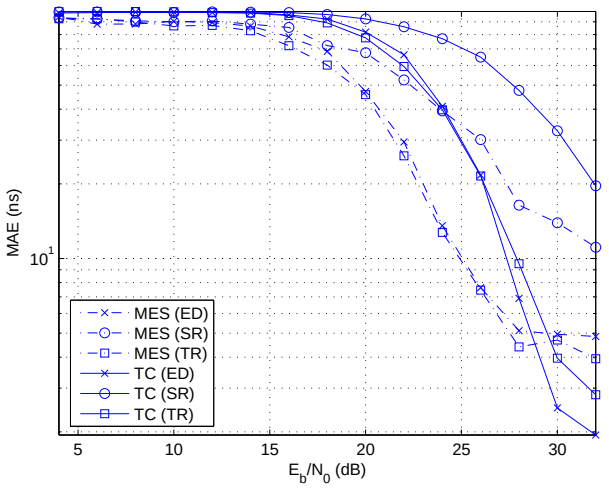

Fig. 10. TOA estimation performances of different transceiver types using MES and TC (CM2, $t_s = T_c = T_b = 1$ns), with timing offset within first energy block.

[7] R. A. Scholtz and J. Y. Lee, "Problems in modeling UWB channels," in *Proc. IEEE Asilomar Conf. Signals, Syst. Computers*, vol. 1, Monterey, CA, Nov. 2002, pp. 706–711.

[8] K. Yu and I. Oppermann, "Performance of UWB position estimation based on time-of-arrival measurements," in *Proc. IEEE Conf. Ultrawideband Syst. Technol. (UWBST)*, Kyoto, Japan, May 2004, pp. 400–404.

[9] R. Fleming, C. Kushner, G. Roberts, and U. Nandiwada, "Rapid acquisition for ultra-wideband localizers," in *Proc. IEEE Conf. Ultrawideband Syst. Technol. (UWBST)*, Baltimore, MD, May 2002, pp. 245–249.

[10] W. Chung and D. Ha, "An accurate ultra wideband (UWB) ranging for precision asset location," in *Proc. IEEE Conf. Ultrawideband Syst. Technol. (UWBST)*, Reston, VA, Nov. 2003, pp. 389–393.

[11] I. Guvenc and Z. Sahinoglu, "Multiscale energy products for TOA estimation in IR-UWB systems," IEEE Global Telecommun. Conf. (GLOBECOM), St. Louis, MO, Dec. 2005, submitted.

[12] Z. Tian and G. B. Giannakis, "A GLRT approach to data-aided timing acquisition in UWB radios – Part I: Algorithms," *IEEE Trans. Wireless Commun.*, 2005 (to appear).

[13] M. H. Chung and R. A. Scholtz, "Comparison of transmitted- and stored-reference systems for ultra-wideband communications," in *Proc. IEEE Military Commun. Conf. (MILCOM)*, Monterey, CA, Oct. 2004.

[14] S. M. Kay, *Fundamentals of Statistical Signal Processing: Detection Theory*. Upper Saddle River, NJ: Prentice Hall, Inc., 1998.

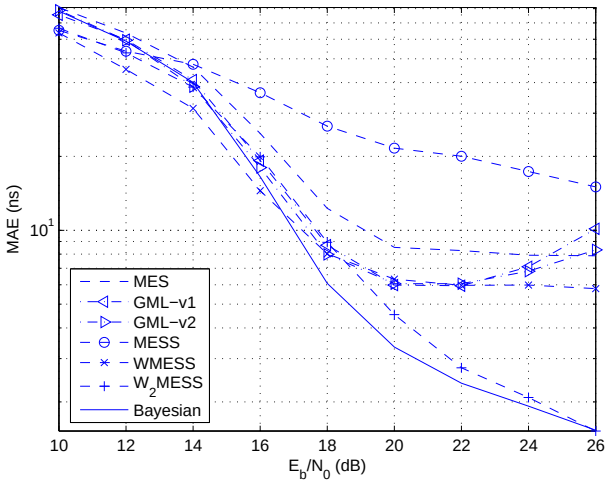

Fig. 11. Performances of different TOA estimators for ED (CM1, $t_s = T_b = 4$ns), with timing offset within first energy block.